Surface Plasmonic Lattice Solitons in Semi-Infinite Graphene Sheet Arrays

Zhouqing Wang, Bing Wang, Hua Long, Kai Wang, and Peixiang Lu

***Abstract*—We investigate the surface plasmonic lattice solitons (PLSs) in semi-infinite graphene sheet arrays. The surface soliton is formed as the surface plasmon polaritons (SPPs) tunneling is inhibited by the graphene nonlinearity, and meanwhile the incident power should be above a threshold value. Thanks to the strong confinement of SPPs on graphene, the effective width of surface PLSs can be squeezed into deep-subwavelength scale of $\sim$0.002λ. The influence of the graphene loss on the surface PLSs is also discussed. Based on the stable propagation of surface PLSs, we find that the light propagation can be switched from the array boundary to the inner graphene sheets by reducing the incident power or increasing the chemical potential of graphene. The study may find promising application in optical switches on deep-subwavelength scale.**

***Index Terms*—Graphene, nonlinear optics, surface solitons.**

I. Introduction

THE optical phenomena supported by the periodic discrete structures such as dielectric waveguide arrays and plasmonic lattices have attracted great interest [1]–[3]. These periodic discrete structures provide a fertile platform for the light to exhibit various novel properties. As the optical phenomena take place with nonlinear effects considered, the light could exhibit more interesting behaviours, including diffraction-free propagation and all-optical control [3]–[5]. The discrete soliton is a typical class of the nonlinear optical phenomena in the periodic discrete structure [6]–[9]. To realize extremely small width of solitons with relatively low input power, ones have paid attention to the solitons formed in plasmonic lattice such as the metal-dielectric arrays instead of dielectric lattices [10]–[13]. The surface plasmon polaritons (SPPs) on metals manifest strong confinement of the light field, which could make the nonlinear effect stimulated readily. In plasmonic lattice, the discrete solitons are known as plasmonic lattice solitons (PLSs). The solitons are formed as the SPPs tunneling is inhibited by nonlinear effect. Usually PLSs are investigated in the infinite (or homogenous) plasmonic lattice [12]–[14]. There is also a type of PLSs existing at the boundary of the truncated plasmonic lattice, which is the surface plasmonic lattice soliton [15]. Compared with the counterparts in the infinite lattice, the surface solitons are unique which require the input power above a threshold value [16]–[19].

Many analogous nonlinear optical phenomena including the discrete solitons, have also been studied in the graphene metamaterials [20]–[25]. In comparison with metals, the SPPs on graphene have superior features including the stronger confinement, more flexible tunability, and lower propagation loss [26]–[33]. Apart from that, graphene itself exhibits strong optical nonlinearity [20], [34], [35]. These features make graphene sheet arrays an ideal substitution of the metallic waveguide arrays for researching plasmonic lattice solitons.

In this work, we shall investigate the surface PLSs in the semi-infinite graphene sheet arrays (GSAs). By comparing with the infinite GSAs where the solitons locate inside the graphene sheets, the surface solitons distribute at the interface of graphene system and an open half-space. Thus there is possibility for the graphene solitons interacting with other materials and being modulated by the external environment. As a result, the surface solitons may find applications in sensors and environment detection. Besides, the surface solitons are easier to excite by an optical coupler than the bulk solitons. At the boundary of the semi-infinite graphene sheet arrays, the graphene nonlinearity excited by the light power above a threshold value balances the SPPs tunneling to form the surface PLSs. Due to the strong confinement of SPPs on graphene, the transverse distribution of the surface PLSs can be compressed into deep-subwavelength scale ($\sim$0.002λ). Recently, Bludov *et al.* studied the dispersion relation of the plasmonic soliton modes in graphene arrays but the loss influence of graphene plasmons is not considered [24]. In this work, we expand the previous study and focus on the practical propagation of surface PLSs in the semi-infinite GSAs at a fixed frequency. We have systematically investigated the field confinement, power threshold, and propagation loss of the surface PLSs. Moreover, the application in optical switches has also been numerically demonstrated. The study may find potential applications in the optical switches, sensors, and optical circuits on deep-subwavelength scale.

Manuscript received January 26, 2017; revised April 10, 2017; accepted May 19, 2017. Date of publication May 24, 2017; date of current version June 19, 2017. This work was supported in part by the 973 Program under Grant 2014CB921301, in part by the National Natural Science Foundation of China under Grants 11304108 and 11674117, in part by the Natural Science Foundation of Hubei Province under Grant 2015CFA040, and in part by the Specialized Research Fund for the Doctoral Program of Higher Education of China under Grant 20130142120091. *(Corresponding author: Bing Wang.)*

Z. Wang, B. Wang, H. Long, and K. Wang are with the School of Physics and the Wuhan National Laboratory for Optoelectronics, Huazhong University of Science and Technology, Wuhan 430074, China (e-mail: 948226642@qq.com; wangbing@hust.edu.cn; longhua@hust.edu.cn; kale_wong@hust.edu.cn).

P. Lu is with the School of Physics and the Wuhan National Laboratory for Optoelectronics, Huazhong University of Science and Technology, Wuhan 430074, China, and also with the Laboratory of Optical Information Technology, Wuhan Institute of Technology, Wuhan 430205, China (e-mail: lupeixiang@hust.edu.cn).

Color versions of one or more of the figures in this paper are available online at http://ieeexplore.ieee.org.

Digital Object Identifier 10.1109/JLT.2017.2707601

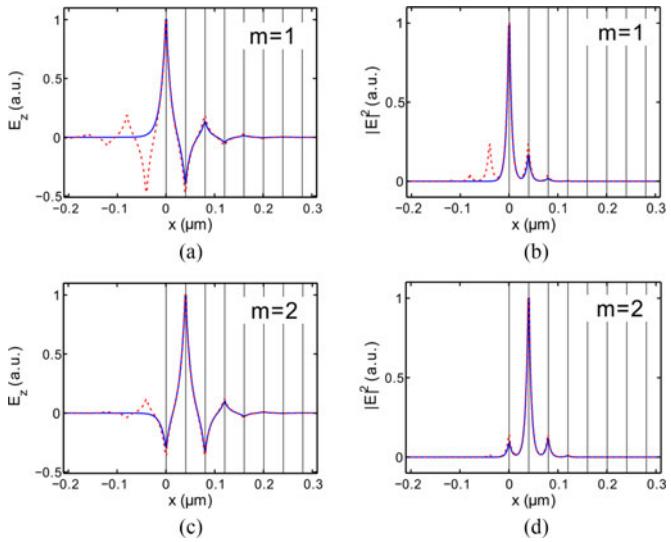

Fig. 1. (a) (b) The normalized tangential electric field (E_z) and the normalized intensity distribution ($|E|^2$) of the surface PLSs for the $m = 1$ mode (blue lines). (c) (d) The normalized tangential electric field (E_z) and the normalized intensity distribution ($|E|^2$) of the surface PLSs for the $m = 2$ mode (blue lines). The black lines stand for the graphene sheets and the red dash lines represent the PLSs in the infinite graphene sheet arrays.

II. Mode Distribution and Propagation of Surface PLSs

We firstly investigate the transverse field distribution and propagation of surface PLSs in the semi-infinite graphene sheet arrays. The structure is shown in Fig. 1, where the semi-infinite graphene sheet arrays ($x > 0$) embedding in the linear dielectric ($\varepsilon_d = 2.25$). The graphene sheets are represented by the black lines and the distance between adjacent graphene sheets is $d = 40$ nm.

Considering the transverse magnetic polarization (TM), we transform the Maxwell's equations into the matrix form [12]

$$\begin{pmatrix} 0 & \dfrac{k_0\varepsilon_r(x)}{\eta_0} \\ \dfrac{\eta_0}{k_0}\dfrac{\partial}{\partial x}\dfrac{1}{\varepsilon_r(x)}\dfrac{\partial}{\partial x} + k_0\eta_0 & 0 \end{pmatrix}\begin{pmatrix} H_y \\ E_x \end{pmatrix} = k_z \begin{pmatrix} H_y \\ E_x \end{pmatrix}, \tag{1}$$

where $\varepsilon_r(x)$ stands for the relative permittivity along the x axis. Equation (1) is aimed at solving the eigen problem. The transverse magnetic field and electric field, H_y and E_x, compose of the eigenvector, while the propagation constant k_z is the eigenvalue. In the calculation, graphene is treated as a thin film with an equivalent thickness $\Delta \approx 1$ nm. Then the relative equivalent permittivity of graphene could be given by $\varepsilon_g = 1 + i\sigma_g\eta_0/(k_0\Delta)$ [20], where η_0 and k_0 are the impendence and propagation constant in vacuum. The nonlinearity of graphene originates from its surface conductivity which can be written as $\sigma_g = \sigma_{g,\text{linear}} + \sigma^{NL}|E_z|^2$. The nonlinear conductivity σ^{NL} is obtained from the general quantum theory of the graphene third-order nonlinear conductivity [36],

$$\sigma^{NL} = \sigma_0^{(3)}(S^{(3/0)} + S^{(2/1)} + S^{(1/2)} + S^{(0/3)}), \tag{2}$$

where $\sigma_0^{(3)} = e^4\hbar {V_F}^2/(4\pi\mu_c^4)$ with μ_c is the chemical potential of graphene and the Fermi velocity $V_F \approx c/300$. $S^{(m/n)}$ is dimensionless and represents the combination of intraband and interband contributions. The term $n = 0$ refers to net intraband contribution and $m = 0$ denotes net interband contribution. The other two terms are due to the combination of both intraband and interband contributions. The detail can be found in the reference [36]. When $n = 0$, the nonlinear conductivity is obtained due to the only contribution of intraband transition ($S^{(3/0)}$) and has the form

$$\sigma^{NL} = -i\frac{3}{8}\frac{e^2}{\pi\hbar^2}\left(\frac{eV_F}{\mu_c\omega}\right)^2\frac{\mu_c}{\omega}, \tag{3}$$

which coincides with the model by [21], [34]. It should be mentioned that the nonlinear surface conductivity could also be depicted by a recently developed non-perturbative model [37], [38] which might be helpful to obtain more accurate results. The linear part of the surface conductivity $\sigma_{g,\text{linear}}(\lambda, \mu_c, \tau)$ is also obtained from the new model [36], which is consistent with the result of Kubo formula [33], [39], where λ is the incident wavelength in air and τ is the momentum relaxation time. Here, these parameters are respectively set as $\lambda = 10\,\mu$m, $\mu_c = 0.16$ eV, $\tau = 0.5$ ps [40]–[42].

Taking the graphene nonlinearity into consideration, (1) turns into a nonlinear eigen problem, which could be solved by using the self-consistent method [43]. We set a Gaussian distribution around the array boundary as initial value for the iterative calculation, where the peak intensity is set as 700 $V^2/\mu m^2$. The transverse field distribution of surface PLSs, namely, the nonlinear eigenmode profile, is obtained as shown in Fig. 1. Here, the loss of graphene is not taken into account at first. It has also been verified that the solutions do not change much even though the loss is included. We denote the nonlinear eigenmode as $m = 1$ or 2 mode when the peak of the intensity profile localizes at the first or second graphene sheet. For the mode of $m = 1$, the tangential electric field (E_z) and the intensity distribution $|E|^2 = |E_x|^2 + |E_z|^2$ are presented (blue lines) in Fig. 1(a) and (b). The transverse field distribution of surface PLS is asymmetric as shown in Fig. 1(b). Due to the boundary effect, the attenuation degree of the intensity amplitude in the uniform dielectric region is a little larger than that in the array. The power and the effective width of surface PLS are respectively given by [13], [44]

$$P = \frac{1}{2}\int \text{Re}(E_x H_y^*)dx, \tag{4}$$

$$w = \sqrt{\int x^2|E|^2dx \Big/ \int |E|^2dx}. \tag{5}$$

For the mode $m = 1$, the surface PLSs have a width of 0.02 μm which is equal to 0.002λ, while the input power is about 89.8 W/m. However in the infinite plasmonic lattice, the effective width is about 0.0031λ under the same input power of 89.8 W/m. The width of the PLS represented by the red dash line is larger than that based on the semi-infinite lattice, as shown in Fig. 1(b). It indicates that the surface PLSs exhibit stronger power confinement in comparison with the PLSs in the infinite graphene sheet arrays.

As for the $m = 2$ mode, the tangential electric field and the intensity distribution are shown in Figs. 1(c) and (d), respectively. Compared with the $m = 1$ mode, the intensity distribu-

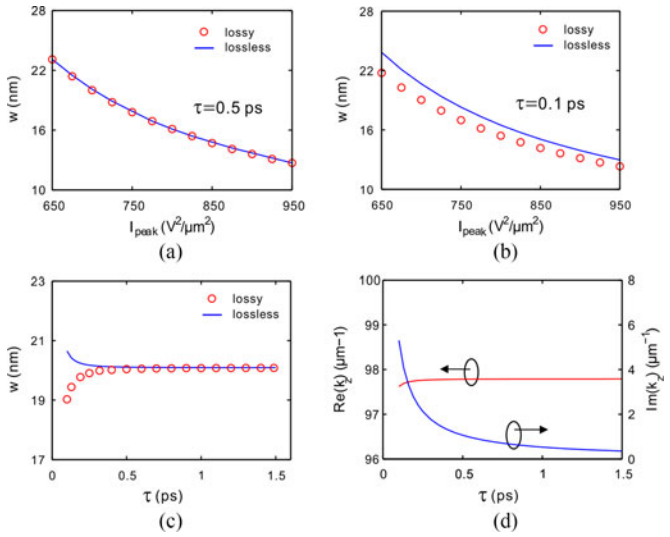

Fig. 2. (a) The effective width of the surface PLSs for the $m = 1$ mode changes with the peak intensity in lossy and lossless cases. (b) As the momentum relaxation time $\tau = 0.1$ ps which is smaller than 0.5 ps, the PLSs width changes with the peak intensity in lossy and lossless cases. (c) As the peak intensity is fixed at $I_{peak} = 700\ \mathrm{V}^2/\mu\mathrm{m}^2$, the PLSs width changes with the momentum relaxation time in lossy and lossless cases. (d) In the loss case, the real and imaginary parts of the propagation constant change with the momentum relaxation time.

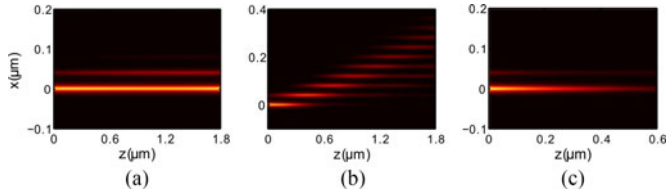

Fig. 3. (a) Propagation of the surface PLSs for $m = 1$ mode in the lossless semi-infinite graphene sheet arrays. (b) Diffraction of SPPs as the nonlinearity is not considered. (c) Actual propagation of the surface PLSs in the lossy semi-infinite graphene sheet arrays.

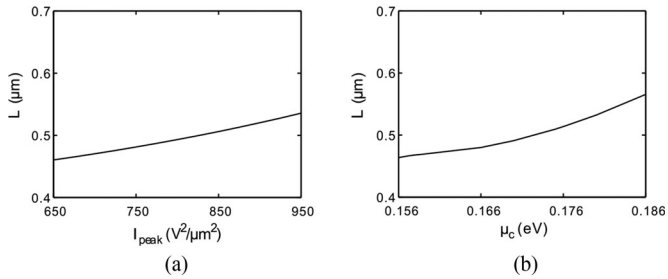

Fig. 4. (a), (b) The decay distance depends on the maximum intensity and the chemical potential, respectively.

tion of $m = 2$ mode tends to be symmetric with the intensity peak moving further into the lattice region. In Fig. 1(d), the effective width of the surface PLS ($m = 2$) is about 0.0046λ and the power approximates to 94.3 W/m. For the PLS in the infinite GSAs, the width are almost the same under the same input power of 94.3 W/m as shown Fig. 1(d).

By comparing the two modes, the width for $m = 2$ mode is about two times larger than that of $m = 1$ mode while the difference between their powers is small. For the same peak intensity, the surface PLS energy could be more concentrated as the distribution is closer to the array boundary. In general, the transverse size of the surface PLS could be squeezed into deep-subwavelength scale (∼0.002λ) with relatively low incident power.

We further study the impact of loss on the width of the surface PLSs presented in Fig. 2. For the surface PLSs presented in Fig. 1(b), we change the peak intensity and obtain the corresponding soliton width in lossy and lossless cases as shown in Fig. 2(a). It shows that the transverse distributions of the surface solitons have little change in the two cases. When the momentum relaxation time is modulated from 0.5 ps to 0.1 ps, the width variation with the peak intensity is shown in Fig. 2(b). The widths in the lossy case are a little smaller than that in lossless case. In general, their differences are about 1 nm. In Fig. 2(c), we further present the width of surface PLSs changes with the momentum relaxation time as the peak intensity is fixed at $I_{\mathrm{peak}} = 700\ \mathrm{V}^2/\mu\mathrm{m}^2$. When the momentum relaxation time is 0.1 ps, the width in lossy case is 1.6 nm smaller than the one in lossless case. As the momentum relaxation time increases, especially larger than 0.3 ps, the widths in lossy and lossless cases converge to the same value about 20 nm. The presence or absence of loss has little effect on the soliton width as τ is larger than 0.3 ps. It is also noteworthy that the momentum relaxation time τ is closely related to the graphene loss [45], [46], which has great effect on the imaginary part of the propagation constant. As shown in Fig. 2(d), the imaginary part of the propagation constant decreases dramatically from 5.3 $\mu\mathrm{m}^{-1}$ to 0.53 $\mu\mathrm{m}^{-1}$ as the momentum relaxation time τ increases from 0.1 ps to 1ps. It also shows that the real part of the propagation constant is hardly influenced by the momentum relaxation time and stays around 97.7 $\mu\mathrm{m}^{-1}$.

To illustrate the propagation of the surface plasmonic lattice solitons, we substitute the nonlinear eigenmode solution into the full Maxwell's equation and simulate the propagation of the mode by using the modified split-step Fourier beam propagation method [12]. In the simulation, we focus on the $m = 1$ mode. As shown in Fig. 3(a), the surface PLS keeps its initial distribution and propagates forward stably, where the loss from graphene is neglected. Assuming that the graphene nonlinear effect is not excited, the light beam will diffuse into the graphene sheet arrays, which is shown in Fig. 3(b). The surface solitons are formed due to the balance between graphene nonlinearity and the SPPs tunneling. Taking the loss from graphene into consideration, we also plot the real propagation of the surface PLS as shown in Fig. 3(c). The decay distance L_{loss} is about 0.47 μm with the propagation constant $k_z = 97.78 + 1.06i\ \mu\mathrm{m}^{-1}$ ($L = 1/2\ \mathrm{Im}(k_z)$). The corresponding SPP wavelength is $\lambda_p = 0.064\,\mu$m. Accordingly, the decay distance is about seven times of the SPP wavelength $L = 7.3\lambda_p$.

As for the actual soliton propagation, we also present the influence of the maximum intensity and the chemical potential on the decay distance in Fig. 4. When the peak intensity increases from 650 $\mathrm{V}^2/\mu\mathrm{m}^2$ to 950 $\mathrm{V}^2/\mu\mathrm{m}^2$, the propagation length decreases slightly from 0.46 μm to 0.54 μm as shown in Fig. 4(a). On the other hand, when the chemical potential increases in

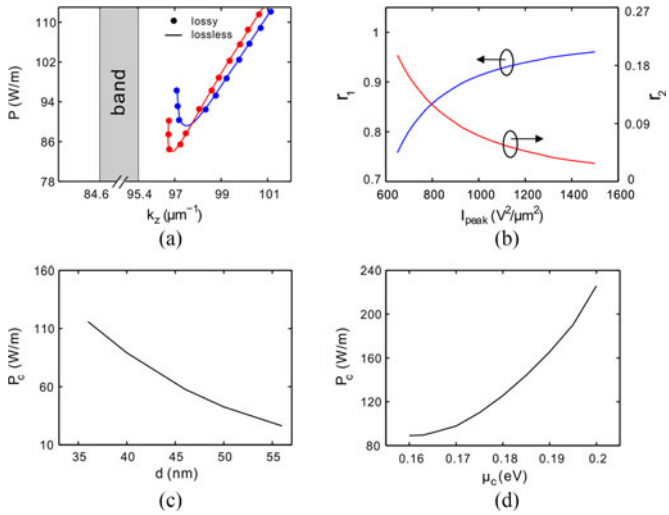

Fig. 5. (a) The relation between the input power and the propagation constant in the lossy and lossless cases respectively. (b) For $m = 1$ mode, the proportions of the energy confined around the first graphene sheet (blue line) and the second sheet (red line). (c) (d) The threshold power of the $m = 1$ mode versus the period of the structure and the chemical potential of graphene.

the small range of 0.156–0.186 eV, the propagation distance increases a little more largely as shown in Fig. 4(b). It should be noted that the chemical potential variation makes the soliton width changed at the same time.

III. Excitation Threshold of Surface PLSs

Now we investigate the properties of surface PLSs including the threshold of exciting power and energy distribution. Firstly, we present the relation between the input power and the propagation constant of surface PLSs in Fig. 5(a), where the propagation band is indicated by shading. Due to the nonlinearity, the localized modes of $m = 1$ and $m = 2$ exsist in the forbidden band which are seperated from the propagation band. In Fig. 5(a), the relations between the input power and the propagation constant in both lossy and lossless cases are analyzed. They are signed by dots and lines respectively and match each other very well. It indicates that the loss has little effect on the threshold for exciting the surface PLSs. The threshold power of $m = 1$ mode is about 89.15 W/m. Below the value, there is no solution for the surface PLSs which concentrate at the first graphene sheet. For the $m = 2$ mode, the threshold power is about 84 W/m, which is smaller than that of the $m = 1$ mode. Combined with the intensity distributions of $m = 1$ and 2 modes as shown in Fig. 1(b) and (d), we find that the threshold power would decrease as the surface PLS distribution gradually shifts to the internal graphene sheets.

Concerning on the surface PLSs of $m = 1$ mode, we proceed to analyze the influence of the light intensity on the energy distribution. The result is shown in Fig. 5(b), where r_1 and r_2 represent the proportions of the surface PLS energy confined in the first and second graphene sheet, respectively. In Fig. 5(b), it is clear that the soliton energy is more concentrated on the first graphene sheet as the peak intensity increases. Specially, when the intensity peak is larger than 950 $V^2/\mu m^2$, there is more than ninety percent of total energy is confined in the first graphene sheet. At the same time, it also indicates that the effective width is correspondingly less than 0.002λ. When the light intensity becomes larger, the induced nonlinear effect will be enhanced. As a result, the surface PLSs could be further squeezed with more energy concentrated on the first graphene sheet.

We also investigate the influence of the structure period and the chemical potential on the threshold power of the $m = 1$ mode. When the chemical potential is fixed at $\mu_c = 0.16$ eV, the threshold power decreases as the structure period increases, as shown in Fig. 5(c). In case the spacing between adjacent graphene sheets increases, the SPPs coupling becomes weak which needs relatively low nonlinear effect to balance. Consequently, the minimum power which is enough to give rise to the surface PLSs should be reduced. On the other hand, due to the great influence of the chemical potential on the material characteristics of the semi-infinite GSAs, we also reveal the influence of the chemical potential of graphene on the threshold power. The result is shown in Fig. 5(d), where the structure period is fixed at $d = 40$ nm. As the chemical potential is modulated in a small range of $\mu_c = 0.16$- 0.2 eV, the threshold power will vary dramatically from 89.2 W/m to 226 W/m. The threshold power is very sensitive to the chemical potential. In general, the larger chemical potential would enhance the SPPs coupling which requires stronger nonlinear effect to balance [22], [26]. Thus, the corresponding threshold power becomes larger.

IV. Application in Optical Switches

In this part, we shall discuss about the application in optical switches by manipulating the SPPs propagation in the semi-infinite GSAs. In order to illustrate the mechanism of optical switches in the actual lossy condition, we set the chemical potential $\mu_c = 0.18$ eV and the momentum relaxation time $\tau = 1$ ps [45], [46]. In Section II, we have demonstrated that the increase of the momentum relaxation time τ would lead to the dramatic decrease of the propagation loss but induce nothing else change of the surface PLSs. In the other hand, the the SPP coupling could be enhanced by increasing the chemical potential. Taking the two aspects into account, we can make SPPs tunnel through a number of graphene sheets in the decay distance by increasing the chemical potential and the momentum relaxation time in a feasible range.

At first, we simulate the actual stable propagation of the surface PLS which is extremely concentrated at the outmost graphene sheet with the peak intensity $I_{peak} = 800$ $V^2/\mu m^2$. The decay distance is about 1 μm. The light beam can propagate stably within the decay distance as shown in Figs. 6(a) and 7(a), which are the same illustrations of the surface PLS propagation. Then we demonstrate how the light beam diffracts from the boundary into the inner graphene sheets as the balance between nonlinearity and SPPs tunneling is destroyed by changing the input power or the chemical potential. The results are shown in Figs. 6 and 7, respectively.

As we reduce the peak intensity from $I_{peak} = 800$ $V^2/\mu m^2$ to $I_{peak} = 300$ $V^2/\mu m^2$, meanwhile the power is also reduced, the light beam would diffuse into the inner sheets as shown in Fig. 6(b). At the output end $z = 0.8\,\mu$m, the intensity peak localizes at the $4th$ graphene sheet. The contrast between the

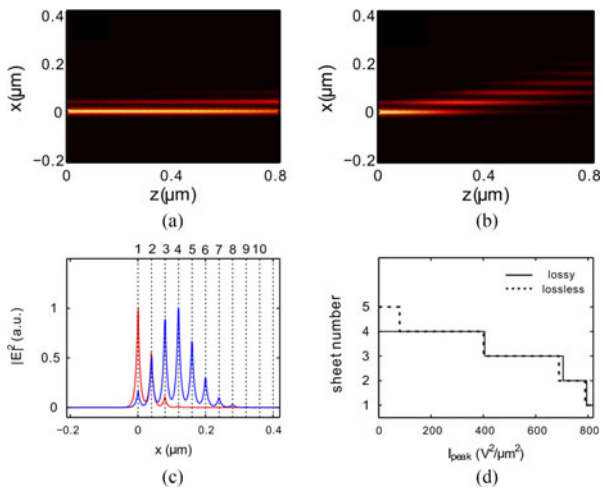

Fig. 6. (a) The actual propagation of surface PLS along the first graphene sheet with the peak intensity $I_{peak} = 800\ \mathrm{V}^2/\mu\mathrm{m}^2$ as the chemical potential is 0.18 eV and the momentum relaxation time $\tau = 1$ ps. (b) The light beam diffuses into the inner sheets of the array as the peak intensity is reduced to $I_{peak} = 300\ \mathrm{V}^2/\mu\mathrm{m}^2$. (c) The comparison of the output intensity distributions of (a) and (b) at $z = 0.8\ \mu$m. (d) As the peak intensity decreases, the output localization of the intensity peak becomes farther away from the array boundary at the output end $z = 0.8\,\mu$m.

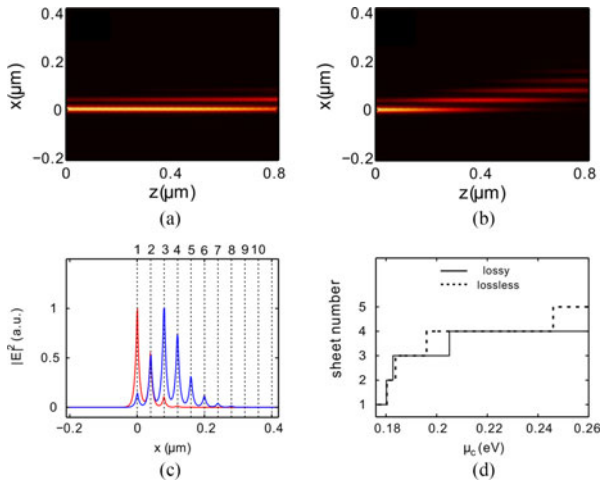

Fig. 7. (a) The actual propagation of surface PLS along the first graphene sheet with the peak intensity $I_{peak} = 800\ \mathrm{V}^2/\mu\mathrm{m}^2$. (b) When the chemical potential is modulated from $\mu_c = 0.18$ eV to $\mu_c = 0.19$ eV, the light beam diffuses into the internal graphene sheets. (c) The comparison of the output intensity distributions of (a) and (b) at $z = 0.8\,\mu$m. (d) As the chemical potential increases, the light output position becomes farther away from the array boundary at the distance $z = 0.8\,\mu$m.

two output intensity distributions is presented in Fig. 6(c). To get more information about how the input power dose influence on the output position, we reduce the peak intensity in turn from $800\ \mathrm{V}^2/\mu\mathrm{m}^2$ to very tiny value. The result is shown in Fig. 6(d). As the peak intensity I_{peak} decreases, the distance between the output position and the array boundary becomes larger. This is because that the light diffraction dominates as the nonlinear effect is weakened by reducing the input power. In Fig. 6(d), we also present the dependence of the output location on the input intensity in the lossless condition, which is represented by the dash line. In the ideal and lossy cases, the optical switch effects are almost the same in the front four sheets except that the light beam could be tuned to one sheet further in the lossless case.

It is known that the chemical potential of graphene can be tuned flexibly by external electric field, magnetic field or gate voltage [26], [27]. From the experimental point of view, one could embed a semiconductor (n^+-Si) layer in the dielectric between graphene and the gate voltage is added between the graphene and semiconductor layers [33]. As the chemical potential increases from $\mu_c = 0.18$ eV to $\mu_c = 0.19$ eV, the light beam diffuses into the array as shown in Fig. 7(b). In the previous section, we have discussed that the increasing chemical potential leads to stronger SPPs coupling. It also indicates that the balance between the graphene nonlinearity and SPP tunneling is broken and the linear diffraction dominates. In Fig. 7(b), the peak of the intensity profile localizes at the 3*th* graphene sheet when the light beam arrives at the output end $z = 0.8\,\mu$m. The intensity distributions of the light beam in Fig. 7(a) and (b) at $z = 0.8\,\mu$m are compared as shown in Fig. 7(c). To illustrate the influence of the chemical potential on the light output position in more detail, we increase the chemical potential from $\mu_c = 0.18$ eV to $\mu_c = 0.26$ eV. The corresponding output positions of the intensity peak are illustrated in Fig. 7(d). As the chemical potential increases, the diffraction becomes in domination and the output location stays farther away from the array boundary. The lossless case is also considered and presented in dash lines in Fig. 7(d). By tuning the chemical potential even in the small range of $\mu_c = 0.18$–0.26 eV, ones can flexibly manipulate the output location of the light.

V. Conclusion

In conclusion, we have investigated the surface plasmonic lattice solitons in semi-infinite graphene sheet arrays. With the prerequisite that the light power is above a threshold value, surface PLSs will be formed as the SPPs tunneling and the graphene nonlinearity reach a balance. Due to the strong confinement of SPPs on graphene, the width of the surface PLSs could reach deep-subwavelength scale ($\sim 0.002\lambda$) with relatively low incident power. The threshold power of surface PLSs can be reduced by increasing the structure period or decreasing the graphene chemical potential. The influence of the graphene loss on the surface PLSs is also discussed. By tuning the chemical potential or the input power, we can also flexibly manipulate the output position of light beam. The study would provide potential application in optical switches on deep-subwavelength scale.

References

[1] D. N. Christodoulides and R. I. Joseph, "Discrete self-focusing in nonlinear arrays of coupled waveguides," *Opt. Lett.*, vol. 13, no. 9, pp. 794–796, Sep. 1988.

[2] H. S. Eisenberg, Y. Silberberg, R. Morandotti, and J. S. Aitchison, "Diffraction management," *Phys. Rev. Lett.*, vol. 85, no. 9, pp. 1863–1866, Aug. 2000.

[3] D. N. Christodoulides, F. Lederer, and Y. Silberberg, "Discretizing light behaviour in linear and nonlinear waveguide lattices," *Nature*, vol. 424, pp. 817–823, Aug. 2003.

[4] Y. Kivshar and G. Agrawal, *Optical Solitons: From Fibers to Photonic Crystals*. New York, NY, USA: Academic, 2003.

[5] Y. V. Kartashov, V. A. Vysloukh, and L. Torner, "Soliton shape and mobility control in optical lattice," *Prog. Opt.*, vol. 52, pp. 63–148, 2009.

[6] Y. S. Kivshar, "Self-localization in arrays of defocusing waveguides," *Opt. Lett.*, vol. 18, no. 14, pp. 1147–1149, Jul. 1993.
[7] H. S. Eisenberg, Y. Silberberg, R. Morandotti, and J. S. Aitchison, "Discrete spatial optical solitons in waveguides arrays," *Phys. Rev. Lett.*, vol. 81, no. 16, Oct. 1998, Art. no. 3383.
[8] J. W. Fleischer, M. Segev, N. K. Efremidis, and D. N. Christodoulides, "Observation of two-dimensional discrete solitons in optically induced nonlinear photonic lattice," *Nature*, vol. 422, pp. 147–150, Mar. 2003.
[9] R. Iwanow *et al.*, "Observation of quadratic solitons," *Phys. Rev. Lett.*, vol. 93, no. 11, Sep. 2004, Art. no. 113902.
[10] A. V. Zayats and I. I. Smolyaninov, "Near-field photonics: Surface plasmon polaritons and localized surface plasmons," *J. Opt. A: Pure Appl. Opt.*, vol. 5, no. 4, pp. S16–S50, Jun. 2003.
[11] W. L. Barnes, A. Dereux, and T. W. Ebbesen, "Surface plasmon subwavelength optics," *Nature*, vol. 424, pp. 824–830, Aug. 2003.
[12] Y. Liu, G. Bartal, D. A. Genov, and X. Zhang, "Subwavelength discrete solitons in nonlinear metamaterials," *Phys. Rev. Lett.*, vol. 99, no. 15, Oct. 2007, Art. no. 153901.
[13] Y. Kou, F. Ye, and X. Chen, "Multiband vector plasmonic lattice solitons," *Opt. Lett.*, vol. 38, no. 8, pp. 1271–1273, Apr. 2013.
[14] F. Ye, D. Mihalache, B. Hu, and N. C. Panoiu, "Subwavelength plasmonic lattice solitons in arrays of metallic nanowires," *Phys. Rev. Lett.*, vol. 104, no. 10, Mar. 2010, Art. no. 106802.
[15] Y. Kou, F. Ye, and X. Chen, "Surface plasmonic lattice solitons," *Opt. Lett.*, vol. 37, no. 18, pp. 3822–3824, Sep. 2012.
[16] K. G. Makris, S. Suntsov, D. N. Christodoulides, and G. I. Stegeman, "Discrete surface solitons," *Opt. Lett.*, vol. 30, no. 18, pp. 2466–2468, Sep. 2005.
[17] Y. V. Kartashov, V. A. Vysloukh, and L. Torner, "Surface gap solitons," *Phys. Rev. Lett.*, vol. 96, no. 7, Feb. 2006, Art. no. 073901.
[18] M. I. Molina, R. A. Vicencio, and Y. S. Kivshar, "Discrete solitons and nonlinear surface modes in semi-infinite waveguide arrays," *Opt. Lett.*, vol. 31, no. 11, pp. 1693–1695, Jun. 2006.
[19] C. R. Rosberg *et al.*, "Observation of surface gap solitons in semi-infinite waveguide arrays," *Phys. Rev. Lett.*, vol. 97, no. 8, Aug. 2006, Art. no. 083901.
[20] M. L. Nesterov, J. Bravo-Abad, A. Y. Nikitin, F. J. Garcia-Vidal, and L. Martin-Moreno, "Graphene supports the propagation of subwavelength optical solitons," *Laser Photon. Rev.*, vol. 7, no. 2, pp. L7–L11, Mar. 2013.
[21] D. A. Smirnova, I. V. Shadrivov, A. I. Smirnov, and Y. S. Kivshar, "Dissipative plasmon-solitons in multilayer graphene," *Laser Photon. Rev.*, vol. 8, no. 2, pp. 291–296, Mar. 2014.
[22] Z. Wang, B. Wang, H. Long, K. Wang, and P. Lu, "Plasmonic lattice solitons in nonlinear graphene sheet arrays," *Opt. Express*, vol. 23, no. 25, pp. 32679–32689, Dec. 2015.
[23] Z. Wang, B. Wang, H. Long, K. Wang, and P. Lu, "Vector plasmonic lattice solitons in nonlinear graphene-pair arrays," *Opt. Lett.*, vol. 41, no. 15, pp. 3619–3622, Aug. 2016.
[24] Y. V. Bludov, D. A. Smirnova, Y. S. Kivshar, N. M. R. Peres, and M. I. Vasilevskiy, "Discrete solitons in graphene metamaterials," *Phys. Rev. B*, vol. 91, no. 4, Jan. 2015, Art. no. 045424.
[25] F. Wang *et al.*, "Asymmetric plasmonic supermodes in nonlinear grapheme multilayers," *Opt. Express*, vol. 25, no. 2, pp. 1234–1241, Jan. 2017.
[26] B. Wang, X. Zhang, F. J. García-Vidal, X. Yuan, and J. Teng, "Strong coupling of surface plasmon polaritons in monolayer graphene sheet arrays," *Phys. Rev. Lett.*, vol. 109, no. 7, Aug. 2012, Art. no. 073901.
[27] J. Christensen, A. Manjavacas, S. Thongrattanasiri, F. H. L. Koppens, and F. J. Garcia de Abajo, "Graphene plasmon waveguiding and hybridization in individual and paired nanoribbons," *ACS Nano*, vol. 6, no. 1, pp. 431–440, Jan. 2012.
[28] Y. Fan, B. Wang, K. Wang, H. Huang, H. Long, and P. Lu, "Plasmonic Zitterbewegung in binary graphene sheet array," *Opt. Lett.*, vol. 40, no. 13, pp. 2945–2948, Jul. 2015.
[29] C. Qin, B. Wang, H. Long, K. Wang, and P. Lu, "Non-reciprocal phase shift and mode modulation in dynamic graphene waveguides," *J. Lightw. Technol.*, vol. 34, no. 16, pp. 3877–3883, Aug. 2016.
[30] H. Huang, S. Ke, B. Wang, H. Long, K. Wang, and P. Lu, "Numerical study on plasmonic absorption enhancement by a rippled grapheme sheet," *J. Lightw. Technol.*, vol. 35, no. 2, pp. 320–324, Jan. 2017.
[31] A. Vakil and N. Engheta, "Transformation optics using graphene," *Science*, vol. 332, pp. 1291–1294, Jun. 2011.
[32] X. Gu, I. Lin, and J. Liu, "Extremely confined terahertz surface plasmon-polaritons in graphene-metal structures," *Appl. Phys. Lett.*, vol. 103, no. 7, Aug. 2013, Art. no. 071103.
[33] P. Y. Chen and A. Alù, "Atomically thin surface cloak using graphene monolayers," *ACS Nano*, vol. 5, no. 7, pp. 5855–5863, Jul. 2011.
[34] S. A. Mikhailov and K. Ziegler, "Nonlinear electromagnetic response of graphene: Frequency multiplication and the self-consistent-field effects," *J. Phys.: Condens. Matter*, vol. 20, no. 38, Aug. 2008, Art. no. 384204.
[35] S. Hong, J. I. Dadap, N. Petrone, P. Yeh, J. Hone, and R. M. Osgood Jr., "Optical third-harmonic generation in graphene," *Phys. Rev. X*, vol. 3, no. 2, Aug. 2013, Art. no. 021014.
[36] S. A. Mikhailov, "Quantum theory of the third-order nonlinear electrodynamic effects of graphene," *Phys. Rev. B*, vol. 93, no. 8, Feb. 2016, Art. no. 085403.
[37] S. A. Mikhailov, "Nonperturbative quasiclassical theory of the nonlinear electrodynamic response of graphene," *Phys. Rev. B*, vol. 95, no. 8, Feb. 2017, Art. no. 045424.
[38] A. Marini, J. D. Cox, and F. J. García de Abajo, "Theory of graphene saturable absorption," *Phys. Rev. B*, vol. 95, no. 12, Mar. 2017, Art. no. 125408.
[39] N. M. R. Peres, "Colloquium: The transport properties of graphene: An introduction," *Rev. Mod. Phys.*, vol. 82, no. 3, pp. 2673–2700, Sep. 2010.
[40] S. Ke, B. Wang, C. Qin, H. Long, K. Wang, and P. Lu, "Exceptional points and asymmetric mode switching in plasmonic waveguides," *J. Lightw. Technol.*, vol. 34, no. 22, pp. 5258–5262, Nov. 2016.
[41] F. Wang, C. Qin, B. Wang, H. Long, K. Wang, and P. Lu, "Rabi oscillations of plasmonic supermodes in graphene multilayer arrays," *IEEE J. Sel. Topics Quantum Electron.*, vol. 23, no. 1, Feb. 2017, Art. no. 4600105.
[42] D. Zhao, Z. Wang, H. Long, K. Wang, B. Wang, and P. Lu, "Optical bistability in defective photonic multilayers doped by graphene," *Opt. Quantum Electron.*, vol. 49, no. 4, Mar. 2017, Art. no. 163.
[43] M. Mitchell, M. Segev, T. H. Coskun, and D. N. Christodoulides, "Theory of self-trapped spatially incoherent light beams," *Phys. Rev. Lett.*, vol. 79, no. 25, pp. 4990–4993, Dec. 1997.
[44] O. Cohen, T. Schwartz, J. W. Fleischer, M. Segev, and D. N. Christodoulides, "Multiband vector lattice solitons," *Phys. Rev. Lett.*, vol. 91, no. 11, Sep. 2003, Art. no. 113901.
[45] H. Huang, B. Wang, H. Long, K. Wang, and P. Lu, "Plasmon-negative refraction at the heterointerface of graphene sheet arrays," *Opt. Lett.*, vol. 39, no. 20, pp. 5957–5960, Oct. 2014.
[46] K. I. Bolotin *et al.*, "Ultrahigh electron mobility in suspended graphene," *Solid State Commun.*, vol. 146, pp. 351–355, Jun. 2008.

Zhouqing Wang received the B.S. degree in optics and electronic information from Jianghan University, Wuhan, China, in 2012. She is currently working toward the Ph.D. degree in the School of Physics, Huazhong University of Science and Technology, Wuhan, China. Her research interests include graphene plasmonics, graphene nonlinearity, and plasmonic lattice solitons.

Bing Wang received the B.S. and Ph.D. degrees in physics from Wuhan University, Wuhan, China, in 2002 and 2007, respectively. He is currently a Professor in the School of Physics and the Wuhan National Laboratory for Optoelectronics, Huazhong University of Science and Technology, Wuhan, China. His current research interests include metal/graphene plasmonics, nanophotonics, nonlinear, and ultrafast optics.

Hua Long received the Ph.D. degree in physics from the Huazhong University of Science and Technology, Wuhan, China, in 2008. She is currently an Associate Professor in the School of Physics, Huazhong University of Science and Technology. Her research interests include theoretical and experimental research for interaction of femtosecond laser and materials.

Kai Wang received the Ph.D. degree in physics from the Huazhong University of Science and Technology, Wuhan, China, in 2011. He is currently an Associate Professor in the School of Physics, Huazhong University of Science and Technology. His research interests include nanophotonics, nonlinear, and ultrafast optics.

Peixiang Lu received the B.S. degree in physics from Peking University, Beijing, China, and the Ph.D. degree from the Shanghai Institute of Optics and Fine Mechanics, Chinese Academy of Sciences, Shanghai, China, in 1987 and 1992, respectively. He is currently a Professor in the School of Physics and the Wuhan National Laboratory for Optoelectronics, Huazhong University of Science and Technology, Wuhan, China. His current research interests include ultrafast optics, laser physics, and nanophotonics. He is a Fellow of the Optical Society of America.